

## **Effect of Undulating Bottom on Wave Interaction with a Floating Flexible Plate Coupled with a Flexible Porous Barrier**

**S. Mandal<sup>1\*</sup>, B. Santosh Kumar<sup>1,2</sup> and A. P. Shashikala<sup>2</sup>**

<sup>1</sup>Ocean Engineering Division, National Institute of Oceanography, Goa- 403004, India

<sup>2</sup>Department of Civil Engineering, National Institute of Technology, Calicut – 673601, India

\* Corresponding author e-mail address: sourav@nio.org

### **Abstract**

In the present study, under the assumption of small amplitude water wave theory and structural response, effect of bed undulation on the wave interaction with a combination of flexible porous barrier and a flexible floating plate, is studied. The flexible porous barrier is modelled using the porous wave maker-theory while the elastic floating plate is modelled using thin plate theory. The physical problem is handled for solution using eigenfunction expansion method by matching pressure and velocity at interface boundaries while finite difference method is used to deal with modified mild-slope equation. In the present study, two types of plate configurations are namely (a) finite plate and (b) semi-infinite plate. To understand the role of undulating seabed, wave and structural parameters, in attenuating wave force and plate deflection, numerical results are computed and compared with available literature. It is found that full wave reflection occurs for certain critical angle and wave force acting on the barrier vanishes for the same critical angle for the semi-infinite plate case while the wave reflection tends to attain maximum value at critical angle for the finite case and these maximum value increases with the increase of plate length. It is observed that less wave reflection occurs for sloping bed profile compare to rest of the bed profile. The study reveals that positioning a barrier between plate and undulated region, helps in the reduction of plate deflection significantly. As special case, wave interaction problem with a finite floating elastic plate is studied experimentally and the experimental result has shown good agreement with the numerical result. The findings of the present study are likely to be of immense help in the design of various types of marine structures for protecting very large floating structures (VLFS). The present theory can be extended to handle large class of acoustic wave interaction problems with flexible porous structures.

**Keywords:** Very large floating structure, Surface gravity waves, Modified mild-slope equation, Flexible porous barrier, Eigenfunction expansion method.

## 1. Introduction

Due to increase in human activities, there is a significant interest to study the gravity wave interaction with very large floating structures for utilization of ocean space for various developmental activities like building offshore floating ports, floating city, and artificial islands. Due to the large structural size, more emphasis is given on the hydroelastic responses of the VLFS, compared to the rigid body motions. However, the associated structural boundary conditions are of higher order than the governing equation, which adds complexities to this kind of problems. Hence, during the past few decades, the interest was to understand the characteristics of the associated eigen-system and analyze wave-VLFS interaction problems through theoretical and experimental investigations for accurate insight into problems.

Floating thin elastic plate model is used widely to model VLFS and the large ice sheet. Squire <sup>[1]</sup> investigated the underlying relationship between VLFS and sea-ice research. Lawrie and Abrahams <sup>[2]</sup> introduced an orthogonal mode-coupling relation for the aquatic wave structure interaction problems. Since then, several authors (see Sahoo et al. <sup>[3]</sup>, Manam et al. <sup>[4]</sup>, Mondal et al. <sup>[5]</sup>, Mohapatra et al. <sup>[6]</sup>) applied orthogonal mode-coupling relation to solve the gravity wave interaction with very large floating structure problems. Hermans <sup>[7]</sup> derived an integro-differential using boundary element method to solve for the flexible plate deflection, which was extended to the floating elastic plates of non-rectangular geometry by Andrianov and Hermans <sup>[8-9]</sup>. Tkacheva <sup>[10]</sup> used Wiener–Hopf technique to deal with wave interaction with floating elastic plate. Watanabe et al. <sup>[11]</sup> provided theoretical background and discussed the design parameters of VLFS. Kohout et al. <sup>[12]</sup> investigated wave propagation beneath a set of elastic plates of arbitrary properties through a series of experiments in a 2D wave tank. Their results satisfied the energy balance condition. Mohapatra et al. <sup>[13]</sup> considered the effect of compressive force in obliquely incident wave interaction with floating plate and found critical compressive forces in different water depths by analyzing the phase and group velocities of the flexural gravity waves. Wang and Tay <sup>[14]</sup> reviewed the role of hydroelasticity and highlighted various mathematical difficulties associated with class of problems associated with VLFS design.

Construction of breakwater close to the VLFS, helps in developing an effective wave protection system and reducing wave-induced drift force for the VLFS (see Ohmatsu <sup>[15]</sup>, Maeda et al. <sup>[16]</sup>, Utsunomiya et al. <sup>[17]</sup> and Hong et al. <sup>[18]</sup>). Perforated wall reduces incoming wave amplitudes by dissipating maximum wave energy. Wang and Ren <sup>[19]</sup> studied hydroelastic responses of wave interaction with a thin flexible porous barrier using the porous wave maker theory developed by Chwang <sup>[20]</sup>. Yip et al. <sup>[21]</sup> used Least Square Approximation method which was initially used by Lee and Chwang <sup>[22]</sup> to deal with the wave interaction with partial barriers. In order to create a tranquility zone near floating

horizontal plate, the challenge is to trap the wave by finding an optimum distance between the structures depending on the incoming wavelength. Bhattacharjee and Soares<sup>[23]</sup> investigated the utility of step type bottom in wave trapping by flexible barrier near a wall. Often multiple barriers are chosen due to their ability to suppress the wave oscillation near protected structure and the gap between two barriers plays a significant role in controlling wave reflection and transmission (see Lo<sup>[24]</sup>, Karmakar et al.<sup>[25]</sup>, Karmakar and Guedes Soares<sup>[26]</sup>). Xiao et al.<sup>[27]</sup> experimented the performance of double-layered perforated walls attached to a VLFS in wave attenuation. They concluded that horizontal motion, mooring force, and wave attenuation are important in VLFS design. Recently, Geng et al.<sup>[28]</sup> studied the influence of the thickness, the porosity and the layout form of the multi-layer perforated plates on the wave absorption efficiency. They found that the efficiency of the wave absorption system doesn't significantly increase after exceeding certain layer number.

However, in all the above mentioned studies, uniform water depth was considered. Over an undulating bottom topography, Massel<sup>[29]</sup> introduced the Galerkin-Eigenfunction method to deal with wave propagation. Porter and Staziker<sup>[30]</sup> improved the accuracy of the mild slope equation approximations by using variational method. They applied continuities of pressure and velocity at the interface of the regions. Chamberlain and Porter<sup>[31]</sup> derived modified mild-slope equation (MMSE) with correct interfacial matching conditions. Since then, several authors applied MMSE to study scattering of flexural and membrane-coupled gravity waves with varying bottom topography (see Bennetts et al.<sup>[32]</sup>, Manam and Kaligatla<sup>[33]</sup>). However, MMSE is non-conservative with respect to wave energy, due to the slope bottom boundary condition. To correct this shortcoming, Athanassoulis and Belibassakis<sup>[34]</sup> developed a consistent couple-mode theory by introducing additional slopping mode in the velocity potential expression and showed that their model improves the convergence of the modal series. Belibassakis and Athanassoulis<sup>[35]</sup> extended the consistent couple-mode theory in the case of obliquely incident waves and studied the hydroelastic analysis of VLFS positioned over undulating regions. Latter, Gerostathis et al.<sup>[36]</sup> extended the work of Belibassakis and Athanassoulis<sup>[35]</sup> to three dimension. Zhu<sup>[37]</sup> used finite difference scheme to solve the MMSE associated with wave interaction with a porous medium. Behera et al.<sup>[38]</sup> investigated wave trapping phenomenon by a combination of porous barrier and rigid wall in the presence of step type bottom topography. They observed that occurrence of optimum reflection increases in case of undulated bed. Kaligatla et al.<sup>[39]</sup>, Behera and Ng<sup>[40]</sup> extended the problem to multiple flexible porous barrier and observed that suitable gap between barriers and sea wall increases the wave reflection significantly in the presence of undulated bottom.

In the present paper, surface gravity wave interaction with a combination of flexible porous barrier and a flexible horizontal plate is investigated in the presence of an undulating bottom bed. The physical problem is formulated under the assumption of small amplitude structural response. Porous wave maker theory and thin plate theory are implemented in the present study in order to model flexible porous barrier and floating elastic plate respectively. Both friction and inertia terms are included in the porous effect parameter. In the presence of undulating bottom, the role of the flexible porous barrier, in the reduction of plate deflection is studied by analyzing the reflection coefficients, surface elevations and different types of bed profiles. Further, as a special case of the main problem, the deflection of the finite floating elastic plate is studied numerically and validated experimentally.

## 2. Mathematical formulation

The problem of oblique wave scattering by the thin flexible porous barrier and an elastic plate is studied in the presence of undulating bottom topography under the assumption of linearized water wave theory and small amplitude structural responses. The problem is formulated in a Cartesian coordinate system with the  $x$ -axis and  $z$ -axis being in the horizontal and vertically upward direction respectively. A flexible porous barrier, extending from seabed to free surface, is placed between the undulated region and the floating plate (as in Fig. 1) to reduce the wave impact on the elastic plate.

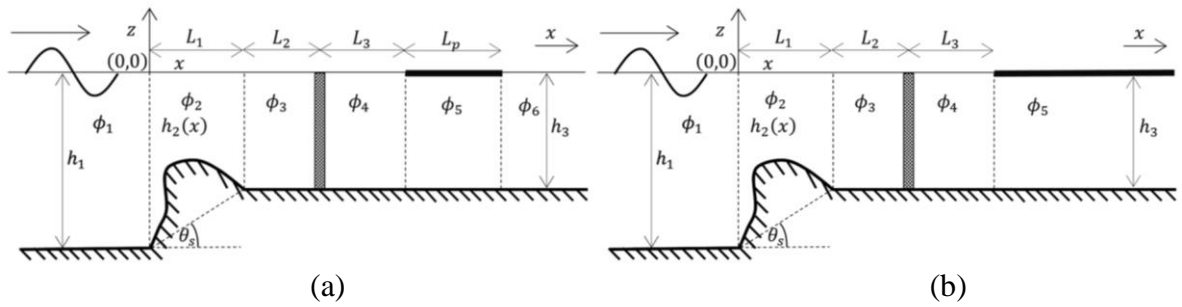


Fig 1: Schematic diagram of (a) finite and (b) semi-infinite elastic plate in the presence of undulating seabed and barrier

The barrier is assumed to be free at the top and fixed at the bottom. Depending on the location of the elastic plate and flexible porous barrier, the fluid domain is divided into sub-domains  $D_1 = -\infty < x \leq 0$ ,

$D_2 = 0 < x \leq x_1$ ,  $D_3 = x_1 < x \leq x_2$ ,  $D_4 = x_2 < x \leq x_3$  along with

$D_5 = x_3 < x < x_4$ ,  $D_6 = x_4 < x < \infty$  where  $x_k = \sum_{i=1}^k L_i$  ( $k=1,2,3,4$ ),  $L_4 = L_p$ , (for finite plate),

$D_5 = x_3 < x < \infty$  where  $x_k = \sum_{i=1}^k L_i$  ( $k=1,2,3$ ), (for semi-infinite plate),

where  $L_p$  is the length of the finite elastic plate. The region 2 contains the undulated bed profiles while the rest of the regions deal with uniform bed. The free surface region is assumed to be of uniform depth of  $h_1$ , extended in the negative  $x$ -direction. The undulated region of variable depth  $h_2(x)$  extends over  $0 < x < L_1$  and the region beyond  $x \geq L_1$  is of uniform depth  $h_3$ . The flexible porous barrier is located at  $x = x_2$  whereas the elastic plate is located at  $x = x_3$ . It is assumed that the fluid is incompressible, inviscid and irrotational in time with angular frequency  $\omega$ . Thus, the velocity potential function exists and has the form  $\Phi_j(x, y, z, t) = \text{Re} \left\{ \phi_j(x, z) e^{-i(\mu_y y + \omega t)} \right\}$ , where  $\mu_y = k_{1,0} \sin \theta$ , and  $k_{1,0}$  being the incident wave number at region 1. The spatial velocity potential  $\phi_j$  ( $j = 1, 2, 3, 4, 5, 6$  for finite plate) and ( $j = 1, 2, 3, 4, 5$  for semi-infinite plate) satisfies the following Laplace equation,

$$\left( \frac{\partial^2}{\partial x^2} + \frac{\partial^2}{\partial z^2} - \mu_y^2 \right) \phi_j = 0, \quad (1)$$

along with the bottom boundary conditions

$$\frac{\partial \phi_2}{\partial z} + \frac{dh_2}{dx} \frac{\partial \phi_2}{\partial x} = 0, \text{ at } z = -h_2(x), \quad 0 < x < L_1, \quad (2)$$

$$\frac{\partial \phi_j}{\partial z} = 0, \text{ at } z = -h_i \text{ for } i = 1, 3, \quad (3)$$

where  $j = 1, 3, 4, 5, 6$  for finite plate and  $j = 1, 3, 4, 5$  for semi-infinite plate. The linearized free surface condition is given by

$$\frac{\partial \phi_j}{\partial z} - L_s \phi_j = 0, \text{ at } z = 0, \quad (4)$$

where  $j = 1, 2, 3, 4, 6$  for finite plate and  $j = 1, 2, 3, 4$  for semi-infinite plate with  $L_s = \omega^2 / g$ , with  $g$  being the acceleration due to gravity. On the other hand, at the plate covered region, the linearized kinematic and dynamic conditions can be expressed as

$$\frac{\partial \eta}{\partial t} = \frac{\partial \Phi_5}{\partial z}, \quad p_s = -\rho \frac{\partial \Phi_5}{\partial t} - \rho g \eta \text{ at } z = 0, \quad (5)$$

with  $\eta(x, t) = \eta_1(x) e^{-i(\mu_y y - \omega t)}$  being the deflection of the floating elastic plate,  $\rho$  being the water density and  $p_s$  being the surface pressure. The plate is assumed to be thin and homogeneous elastic

material with thickness  $t_p$  and mass density  $\rho_p$ . Now, from Eq. (5), the dynamic pressure exerted on the plate can be written as

$$p_s = EI_p \nabla_{xy}^4 \eta + m_p \frac{\partial^2 \eta}{\partial t^2} \text{ at } z=0, \quad x_3 < x < x_4 \text{ (for finite plate), } x > x_3 \text{ (for semi-infinite plate),} \quad (6)$$

where  $\nabla_{xy}^2 = \frac{\partial^2}{\partial x^2} + \frac{\partial^2}{\partial y^2} = \frac{\partial^2}{\partial x^2} - \mu_y^2$ , flexural rigidity of the plate  $EI_p = Et_p^3 / [12(1-\nu_p^2)]$ , with  $E$  being the Young's modulus,  $\nu_p$  being Poisson's ratio and the mass of the plate  $m_p = \rho_p t_p$ . Now, substituting Eq. (5) in Eq. (6) gives,

$$EI_p \nabla_{xy}^4 \eta + m_p \frac{\partial^2 \eta}{\partial t^2} = -\rho \frac{\partial \Phi_5}{\partial t} - \rho g \eta. \quad (7)$$

Now, using  $\nabla_{xy}^2 = -\frac{\partial^2}{\partial z^2}$  and  $\frac{\partial \eta}{\partial t} = \frac{\partial \Phi_5}{\partial z}$  in Eq. (7), yields,

$$\left( D \frac{\partial^4}{\partial z^4} + 1 \right) \frac{\partial \phi_5}{\partial z} - K \phi_5 = 0 \text{ at } z=0, \quad (8)$$

where  $D = EI_p / (\rho g - m_p \omega^2)$ ,  $K = \rho \omega^2 / (\rho g - m_p \omega^2)$ . It is assumed that the plate satisfies any one of the following edge conditions at  $x = x_3$ ,  $x = x_4$  (for finite plate) and  $x = x_3$  (for semi-infinite plate),

(a) Free edge: bending moment and shear force are zero,

$$\left( \frac{\partial^2}{\partial x^2} - \nu_p \mu_y^2 \right) \frac{\partial \phi_5}{\partial z} = 0, \quad \left\{ \frac{\partial^2}{\partial x^2} - (2 - \nu_p) \mu_y^2 \right\} \frac{\partial^2 \phi_5}{\partial x \partial z} = 0 \quad (9a)$$

(b) Simply supported edge: displacement and bending moment are zero,

$$\frac{\partial \phi_5}{\partial z} = 0, \quad \left\{ \frac{\partial^2}{\partial x^2} - \nu_p \mu_y^2 \right\} \frac{\partial \phi_5}{\partial z} = 0 \quad (9b)$$

(c) Fixed edge: slope and displacement are zero,

$$\frac{\partial^2 \phi}{\partial x \partial z} = 0, \quad \frac{\partial \phi}{\partial z} = 0 \quad (9c)$$

Koley et al. <sup>[41]</sup> found that the surface-piercing barriers (fixed at top and free at bottom) are efficient in wave blocking over the bottom-standing barriers due to higher wave energy concentration near free surface. However, there is great engineering challenges associated in fixing top end of the barrier.

Moreover, surface piercing barrier is good option for deep water and where sea bed is not suitable for barrier foundation. Since the present study is focused on rigid bed and intermediate water depth, the bottom standing flexible porous barrier preferred here. The barrier is positioned between the plate and undulated region to reduce the wave impact on the elastic plate. The advantages of this kind of barrier is that when wave passes through the porous barrier, it loses much of its energy due to friction of the barrier while part of the energy is used to deform the barrier. Hence, the bottom standing flexible porous barrier is kept fixed at the bottom (i.e., deflection and slope are zero) and free at the top (i.e., bending moment and shear force becomes zero). The flexible porous barrier is modelled using the porous wave maker-theory (see Chwang<sup>[20]</sup>). The interface boundary condition on the flexible porous barrier surface (as in Mandal et al.<sup>[42]</sup>) is given by

$$\frac{\partial \phi_3}{\partial x} = \frac{\partial \phi_4}{\partial x} = ik_0 G(\phi_3 - \phi_4) - i\omega \xi(z) \text{ at } x = x_2, \quad -h_3 < z < 0, \quad (10)$$

where  $G$  is the complex porous-effect parameter as in Yu and Chwang<sup>[43]</sup> and the complex deflection amplitude  $\xi(z)$  is given by

$$EI_b \left( \frac{d^2}{dz^2} - \mu_y^2 \right)^2 \xi + Q \left( \frac{d^2}{dz^2} - \mu_y^2 \right) \xi - m_b \omega^2 \xi = i\omega \rho (\phi_3 - \phi_4) \text{ at } x = x_2, \quad -h_3 < z < 0, \quad (11)$$

where  $EI_b = Et_b^3 / [12(1 - \nu_b^2)]$  being the flexural rigidity and  $Q$  being the compressive force of the flexible porous barrier,  $\nu_b$  being the Poisson's ratio, mass of the barrier per unit length  $m_b = \rho_b t_b$ , with  $\rho_b$  being the density of porous barrier. The edge conditions of the flexible porous barrier are given by

$$\xi = \frac{d\xi}{dz} = 0 \text{ at } z = -h_3, \quad (11)$$

$$\left( \frac{d^2}{dz^2} - \nu_b \mu_y^2 \right) \xi = 0, \quad \left[ EI_b \left\{ \frac{d^2}{dz^2} - (2 - \nu_b) \mu_y^2 \right\} \frac{d}{dz} + Q \frac{d}{dz} \right] \xi = 0 \text{ at } z = 0. \quad (12)$$

Finally, the continuity of pressure and normal velocity near the interfaces yield,

$$\text{Region 1 and 2: } \phi_1 = \phi_2, \quad \frac{\partial \phi_1}{\partial x} = \frac{\partial \phi_2}{\partial x} \text{ at } x = 0, \quad -h_1 < z < 0, \quad (13a)$$

$$\text{Region 2 and 3: } \phi_2 = \phi_3, \quad \frac{\partial \phi_2}{\partial x} = \frac{\partial \phi_3}{\partial x} \text{ at } x = x_1, \quad -h_3 < z < 0, \quad (13b)$$

$$\text{Region 4 and 5: } \phi_4 = \phi_5, \quad \frac{\partial \phi_4}{\partial x} = \frac{\partial \phi_5}{\partial x} \text{ at } x = x_3, \quad -h_3 < z < 0. \quad (13c)$$

Only for finite plate:

$$\text{Region 5 and 6: } \phi_5 = \phi_6, \quad \frac{\partial \phi_5}{\partial x} = \frac{\partial \phi_6}{\partial x} \text{ at } x = x_4, \quad -h_3 < z < 0. \quad (13d)$$

### 3. Method of solution

Now, substituting bottom boundary condition Eq. (3), free surface conditions Eq. (4) and plate cover condition Eq. (8) as appropriate, in Laplace equation Eq. (1), the velocity potential can be expressed as

$$\phi_1(x, z) = I_0 e^{i\mu_{4,0}x} Z_{1,0}(z) + \sum_{n=0}^{\infty} R_n e^{-i\mu_{1,n}x} Z_{1,n}(z) \text{ for } x \in D_1, \quad (14a)$$

$$\phi_2(x, z) = \sum_{n=0}^{\infty} \psi_n(x) Z_{2,n}(h_2(x), z), \text{ for } x \in D_2, \quad (14b)$$

$$\phi_3(x, z) = \sum_{n=0}^{\infty} (A_{1,n} e^{i\mu_{3,n}x} + A_{2,n} e^{-i\mu_{3,n}x}) Z_{3,n}(z) \text{ for } x \in D_3, \quad (14c)$$

$$\phi_4(x, z) = \sum_{n=0}^{\infty} (B_{1,n} e^{i\mu_{3,n}x} + B_{2,n} e^{-i\mu_{3,n}x}) Z_{3,n}(z) \text{ for } x \in D_4, \quad (14d)$$

for finite plate:

$$\phi_5(x, z) = \sum_{n=0, I, II, III, IV}^{\infty} (C_{1,n} e^{iq_n x} + C_{2,n} e^{-iq_n x}) F_n(z) \text{ for } x \in D_5, \quad (14e)$$

$$\phi_6(x, z) = \sum_{n=0}^{\infty} T_n e^{i\mu_{3,n}x} Z_{3,n}(z) \text{ for } x \in D_6, \quad (14f)$$

for semi-infinite plate:

$$\phi_5(x, z) = \sum_{n=0, I, II, III, IV}^{\infty} T_n e^{iq_n x} F_n(z) \text{ for } x \in D_5, \quad (14g)$$

where  $I_0 = -igH_0 / (2\omega)$  and the depth-dependent function  $Z_{1,n}(z)$ ,  $Z_{2,n}(h_2(x), z)$ ,  $Z_{3,n}(z)$  (for  $n = 0, 1, 2, \dots$ ) and  $F_n(z)$  (for  $n = 0, I, II, 1, 2, \dots$ ) are given by  $Z_{1,n}(z) = \frac{\cosh k_{1,n}(h_1 + z)}{\cosh k_{1,n}h_1}$ ,



$$Z_{2,n}(h_2(x), z) = \frac{\cosh k_{2,n}(h_2(x) + z)}{\cosh k_{2,n}h_2(x)}, Z_{3,n}(z) = \frac{\cosh k_{3,n}(h_3 + z)}{\cosh k_{3,n}h_3} \text{ and } F_n(z) = \frac{\cosh p_n(h_3 + z)}{\cosh p_n h_3}, \text{ with}$$

$H_0$  being the incident wave height and  $\mu_{1,n} = \sqrt{k_{1,n}^2 - \mu_y^2}$ ,  $\mu_{3,n} = \sqrt{k_{3,n}^2 - \mu_y^2}$  and  $p_n = \sqrt{q_n^2 - \mu_y^2}$ . The wave numbers  $k_{l,n}$ 's ( $l=1,3$ ) satisfy the dispersion relation  $\omega^2 = gk_{l,n} \tanh k_{l,n}h$  where  $k_{l,0}$  is the real root and  $k_{l,n}$ 's ( $n > 0$ ) are purely imaginary roots. However, it is assumed that, in Eq. (14b),  $k_{2,n}$ 's satisfies  $\omega^2 = gk_{2,n} \tanh k_{2,n}h_2$  with  $k_{2,0}$  being the real root and  $k_{2,n}$ 's ( $n > 0$ ) are purely imaginary roots.

The wave numbers for the plate-covered region,  $p_n$ 's satisfy the relation  $K = p_n(Dp_n^4 + 1) \tanh p_n h_3$  where  $p_0$  is the real root,  $p_I (= p_{II}^*)$ ,  $p_{III} (= p_{IV}^*)$  are complex roots with '\*' denoting the complex conjugate and  $p_n$ 's ( $n > 0$ ) are purely imaginary roots. The eigenfunctions in Eq. (14), satisfy the

$$\text{relation } \langle Z_{l,m}(z), Z_{l,n}(z) \rangle = 0, (m \neq n) \quad \text{where} \quad \langle Z_{l,m}(z), Z_{l,n}(z) \rangle = \int_{-h_l}^0 Z_{l,m}(z) Z_{l,n}(z) dz,$$

( $l=1,3; m,n=0,1,2,\dots$ ). In Eqs. (14a) - (14g), the unknown coefficients  $R_n, A_{1,n}, A_{2,n}, B_{1,n}, B_{2,n}, C_{1,n}, C_{2,n}$  and  $T_n$ , are to be determined using the conditions prescribed on various boundaries for appropriate structural configuration.

### 3.1. Barrier region

Now, applying the orthogonal properties of eigenfunctions in the continuity of velocity and porous boundary conditions at  $x = x_2$ , as in Eq. (10), the followings are derived.

$$A_{1,m} e^{i\mu_{3,m}x} - A_{2,m} e^{-i\mu_{3,m}x} - B_{1,m} e^{i\mu_{3,m}x} + B_{2,m} e^{-i\mu_{3,m}x} = 0 \quad (15)$$

$$\left\{ \left[ (i\mu_{3,m} - ik_0 G) A_{1,m} + ik_0 G B_{1,m} \right] e^{i\mu_{3,m}x} + \left[ -(i\mu_{3,m} + ik_0 G) A_{2,m} + ik_0 G B_{2,m} \right] e^{-i\mu_{3,m}x} \right\} \int_{-h_2}^0 Z_{3,m}^2 dz = -i\omega \int_{-h_2}^0 \xi(z) Z_{3,m} dz. \quad (16)$$

The horizontal displacement profile  $\xi(z)$  in Eq. (16), can be derived by solving the equation of motion as in Eq. (11),

$$\xi(z) = \sum_{k=1}^4 v_k U_k + i\omega \rho \sum_{n=0}^N (\psi_3 - \psi_4) r_n Z_{3,n}, \quad (17)$$

$$\text{with } U_1 = \frac{\cosh(u_1 z)}{\cosh(u_1 h_3)}, U_2 = \frac{\sinh(u_2 z)}{\sinh(u_2 h_3)}, U_3 = \frac{\cos(u_3 z)}{\cos(u_3 h_3)}, U_4 = \frac{\sin(u_4 z)}{\sin(u_4 h_3)},$$

$r_n = \{EI_b \mu_{3,n}^4 + Q \mu_{3,n}^2 - m_b \omega^2\}^{-1}$ , where  $u_n$ 's being the roots of the characteristic equation

$$EI_b (u_n^2 - \mu_y^2)^2 + Q(u_n^2 - \mu_y^2) - m_b \omega^2 = 0, \text{ with } u_n = i u_n \text{ for } n=3,4, \text{ and } v_k \text{ are arbitrary constants.}$$

Now, substitution of Eq. (17) in Eq. (16), yields,

$$\begin{aligned} & \left[ (i\mu_{3,m} - ik_0 G - \omega^2 \rho r_m) A_{1,m} + (ik_0 G + \omega^2 \rho r_m) B_{1,m} \right] e^{i\mu_{3,m} x} a_{3,m} \\ & + \left[ -(i\mu_{3,m} + ik_0 G + \omega^2 \rho r_m) A_{2,m} + (ik_0 G + \omega^2 \rho r_m) B_{2,m} \right] e^{-i\mu_{3,m} x} a_{3,m} + i\omega \int_{-h_3}^0 \left( \sum_{k=1}^4 v_k U_k \right) Z_{3,m} dz = 0, \end{aligned} \quad (18)$$

$$\text{where } a_{3,m} = \int_{-h_3}^0 Z_{3,m}^2 dz.$$

### 3.2. Plate covered region

In this section, for clarity, the motion equation for the two types of plate configurations are discussed in two different subsections.

#### 3.2.1. Finite plate

In the case of finite plate, substitution of  $\phi_4$  and  $\phi_5$  from Eqs. (14d)-(14e) in the continuity of pressures and normal velocity conditions Eq. (13c), and application of orthogonality of eigenfunction  $Z_{3,n}(z)$  at  $x = x_3$ , yields,

$$\left( B_{1,m} e^{i\mu_{3,m} x} + B_{2,m} e^{-i\mu_{3,m} x} \right) a_{3,m} - \sum_{n=0,I,II}^{\infty} \left( C_{1,n} e^{iq_n x} + C_{2,n} e^{-iq_n x} \right) \int_{-h_3}^0 Z_{3,m} F_n dz = 0, \quad (19a)$$

$$\left( B_{1,m} e^{i\mu_{3,m} x} - B_{2,m} e^{-i\mu_{3,m} x} \right) \mu_{3,m} a_{3,m} - \sum_{n=0,I,II}^{\infty} \left( C_{1,n} e^{iq_n x} - C_{2,n} e^{-iq_n x} \right) q_n \int_{-h_3}^0 Z_{3,m} F_n dz = 0. \quad (19b)$$

Similarly, substituting  $\phi_5$  and  $\phi_6$  from Eqs. (14e)- (14f) in Eq. (13d) and used of orthogonality of eigenfunction  $Z_{3,n}(z)$  at  $x = x_4$ , yields,

$$T_m e^{-i\mu_{3,m} x} a_{3,m} - \sum_{n=0,I,II}^{\infty} \left( C_{1,n} e^{iq_n x} + C_{2,n} e^{-iq_n x} \right) \int_{-h_3}^0 Z_{3,m} F_n dz = 0, \quad (20a)$$

$$T_m e^{-i\mu_{3,m}x} \mu_{3,m} a_{3,m} + \sum_{n=0,I,II}^{\infty} (C_{1,n} e^{iq_n x} - C_{2,n} e^{-iq_n x}) q_n \int_{-h_3}^0 Z_{3,m} F_n dz = 0. \quad (20b)$$

### 3.2.2. Semi-infinite plate

In the semi-infinite plate covered region, substitution of  $\phi_4$  and  $\phi_5$  from Eqs. (14d) and (14g) in Eq. (13c) and applying orthogonal properties of eigenfunction  $Z_{3,n}(z)$  near the interface  $x = x_3$ , yields,

$$(B_{1,m} e^{i\mu_{3,m}x} + B_{2,m} e^{-i\mu_{3,m}x}) a_{3,m} - \sum_{n=0,I,II}^{\infty} T_n e^{-iq_n x} \int_{-h_3}^0 Z_{3,m} F_n dz = 0, \quad (21a)$$

$$(B_{1,m} e^{i\mu_{3,m}x} - B_{2,m} e^{-i\mu_{3,m}x}) \mu_{3,m} a_{3,m} + \sum_{n=0,I,II}^{\infty} T_n q_n e^{-iq_n x} \int_{-h_3}^0 Z_{3,m} F_n dz = 0. \quad (22b)$$

### 3.3. Undulated bed region

Now, the infinite series Eq. (14b) is substituted in Laplace equation after truncating  $N$  terms. The following modified mild-slope equation (MMSE) (as in Zhu <sup>[34]</sup>) for the region  $D_2$ , is derived as

$$\begin{aligned} \frac{d^2 \psi_m}{dx^2} + \frac{\partial a_{2,m}}{\partial h_2} \frac{S_c}{a_{2,m}} \frac{d\psi_m}{dx} + \frac{S_c}{a_{2,m}} \sum_{n=0}^N (b_{nm} - b_{mn}) \frac{d\psi_n}{dx} \\ + \frac{1}{a_{2,m}} \sum_{n=0}^N \left\{ b_{nm} \frac{d^2 h_2}{dx^2} + c_{nm} (S_c)^2 + a_{2,m} \mu_{2,n}^2 \right\} \psi_n = 0, \end{aligned} \quad (23)$$

where the coefficients  $a_m$ ,  $b_{nm}$ ,  $c_{nm}$  and  $S_c$  are given by

$$a_{2,m} = \int_{-h_2}^0 Z_{2,m}^2 dz, \quad b_{nm} = \int_{-h_2}^0 Z_{2,m} \frac{\partial Z_{2,n}}{\partial h_2} dz, \quad c_{nm} = \frac{db_{nm}}{dh_2} - \int_{-h_2}^0 \frac{\partial Z_{2,n}}{\partial h_2} \frac{\partial Z_{2,m}}{\partial h_2} dz \quad \text{and} \quad S_c = \frac{dh_2}{dx}.$$

By applying orthogonal properties of eigenfunctions, in Eq. (13a), the following equation can be derived

$$a_{1,m} \left( \frac{\partial \psi_m}{\partial x} \right)_{x=0} + i\mu_{1,m} a_{1,m} \psi_m + S_c \sum_{n=0}^N b_{nm} \psi_n = 2i\delta_{0m} a_{1,m} \mu_{1,m} I_0, \quad \text{at } x=0, \quad (24)$$

where  $a_{1,m} = \int_{-h_1}^0 Z_{1,m}^2 dz$  and  $\delta_{0m}$  being the Kronecker delta. Now, proceeding similarly, using interface

matching conditions in Eq. (13b), the following can be derived,

$$a_{3,m} \left( \frac{\partial \psi_m}{\partial x} \right)_{x=x_1} - i\mu_{3,m} a_{3,m} \psi_m + S_c \sum_{n=0}^N b_{nm} \psi_n = -2ia_{3,m} \mu_{3,m} A_{2,m} e^{-i\mu_{3,m}x}, \text{ at } x = x_1. \quad (25)$$

To solve the modified mild-slope equation Eq. (23), finite difference scheme is applied along with the boundary conditions Eqs. (24) - (25). The undulating domain  $[0, x_1]$  is divided into  $M$  number of equal segments. Forward-difference formula is applied at left boundary node  $x=0$ , while backward-difference formula is applied at the right boundary node  $x = L_1$ . The Central-difference formula is applied to derivatives except derivatives at endpoints.

However, it is important to note that in the present work, the Eq. (14b) is slowly convergent and MMSE is non-conservative with respect to wave energy (see Athanassoulis and Belibassakis<sup>[34]</sup>), due to the slope bottom boundary condition. However, to make conservative and accelerate the convergences, an additional slopping-bottom mode  $\psi_{-1}(x)Z_{2,-1}(h_2(x), z)$  can be added in Eq. (14b) where  $Z_{2,-1}(h_2(x), z)$  being any smooth  $z$ -function in  $[-h_2(x), 0]$  satisfies the following conditions (see Athanassoulis and Belibassakis<sup>[34]</sup>)

$$\left. \frac{\partial Z_{2,-1}}{\partial z} - L_s Z_{2,-1} \right|_{z=0,x} = 0, \quad \left. \frac{\partial Z_{2,-1}}{\partial z} \right|_{z=-h_2(x),x} = 1. \quad (26)$$

The following end conditions can be imposed due to the additional slopping-bottom amplitude  $\psi_{-1}(x)$  and the final system of equations can be solved by following present procedure.

$$\psi_{-1}(0) = \psi_{-1}(x_1) = 0, \quad \psi'_{-1}(0) = \psi'_{-1}(x_1) = 0. \quad (27)$$

Now, using prescribed finite difference scheme, in Eqs. (23) - (25), and Eqs. (9), (11)-(12), (15), (18) with (19)-(20) for finite plate case, yield following system of  $(N+1)(M+7)+4+4$  equations

$$X\vec{Y} = \vec{H} \quad (28)$$

where  $Y = \{R_n, \psi_n^m, A_{1,n}, A_{2,n}, B_{1,n}, B_{2,n}, C_{1,j}, C_{2,j}, v_1, v_2, v_3, v_4, T_n\}$  is unknown column vector ( $m=1, 2, 3, \dots, (M+1)$ ;  $n=1, 2, 3, \dots, N+1$ ;  $j=1, I, II, 2, 3, \dots, N+1$ ) is to be determined. Similarly, for semi-infinite plate case, instead of Eqs. (19)-(20), Eq. (21) is considered and system of  $(N+1)(M+7)+4+2$  equations, is obtained where in Eq. (23),

$Y = \{R_n, \psi_n^m, A_{1,n}, A_{2,n}, B_{1,n}, B_{2,n}, v_1, v_2, v_3, v_4, T_j\}$  is unknown vector ( $m=1, 2, 3, \dots, (M+1)$ ;  $n=1, 2, 3, \dots, N+1$ ;  $j=1, I, II, 2, 3, \dots, N+1$ ) is to be determined.

### 3.4. Special Cases

In this subsection, several special cases of the formulated problem are derived for various structural configurations.

#### 3.4.1. Floating semi-infinite elastic plate in the presence of undulating bottom bed

In this case, the barrier is removed. Hence, the velocity and pressure will be continuous along the interface of 3<sup>rd</sup> and 4<sup>th</sup> region. Proceeding in a similar fashion as in previous section, the problem can be solved considering the following interface condition instead of Eq. (10),

$$\phi_3 = \phi_4. \quad (24)$$

#### 3.4.2. Floating semi-infinite elastic plate without the presence of undulating bottom bed

In this case, the undulating bottom and barrier are eliminated. Hence, the physical problem can be formulated considering  $h_1 = h_2 = h_3$  (see Sahoo et al. [3]). Proceeding in a similar fashion as previous, the problem can be solved using the following condition,

$$\phi_3 = \phi_4 \text{ and } \frac{dh_2}{dx} = 0. \quad (25)$$

#### 3.4.3. Floating finite elastic plate without presence of undulating bottom bed

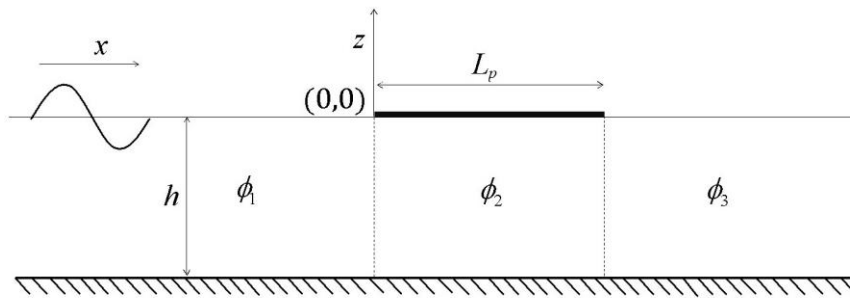


Fig 2: Schematic diagram of wave interaction with finite elastic plate

In this section, as a special case of the formulated problem for finite plate case, wave interaction with a floating finite elastic plate without the presence of undulating bottom bed, which was previously studied by Wu et al. [44], can be derived. For clarity, schematic diagram of wave interaction with finite elastic plate is shown in Fig. 2. Here, the fluid domain is divided into three regions where region 1 is extended in the negative  $x$ -direction, region 2 namely plate covered region starts from origin and region

3 extends in the positive  $x$ -direction beyond  $x = L_p$ . The plate is considered to be floating freely on the water surface of uniform depth  $h = h_1 = h_3$ . The linearized bottom, free surface boundary conditions of the fluid domain and edge conditions of the plate are same as in previous section with  $\theta = 0^0$ . To avoid repetition, detailed mathematical formulation is not provided here. However, to validate the theoretical results of this special case, an experiment is carried out in a wave flume of size  $40m \times 2m \times 2m$  in a water depth of  $1.4m$  at National Institute of Technology Calicut, India.

### Experimental setup

Schematic diagram of the experimental setup is shown in Fig 3.

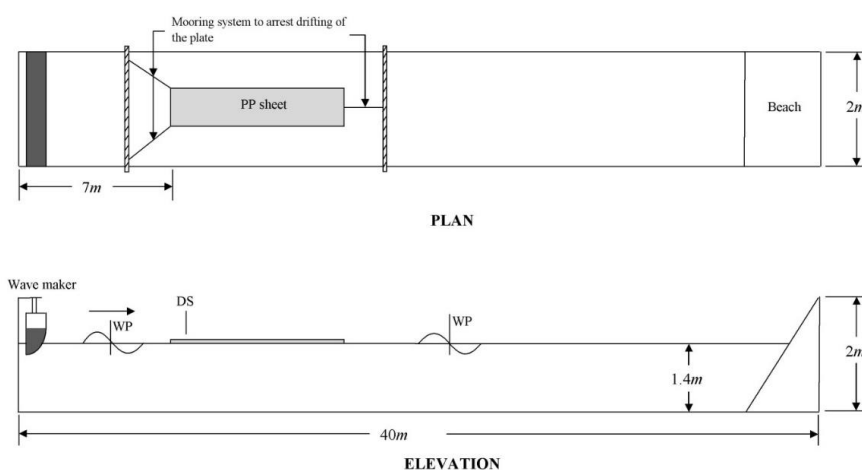


Fig 3: Schematic diagram of the experimental setup

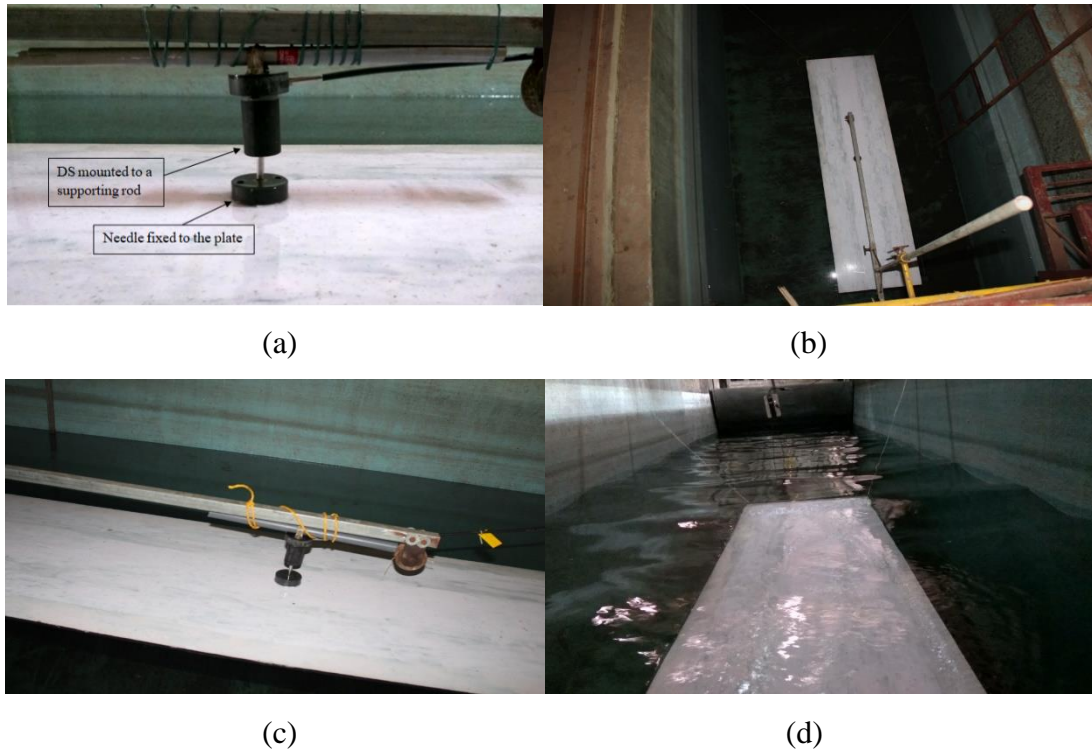


Fig 4: (a) Arrangement of the displacement sensor on the plate, (b) Top view of the floating plate, (c) Side view of the floating plate and (d) Action of waves on the plate

Froude's model law is used extensively in the problems associated with waves because inertia and gravitation are the predominant forces in such systems. The wave height, wavelength and water depth scale linearly ( $1/\lambda$ ) in a Froude model. The time and wave period scale are  $1/\sqrt{\lambda}$ . The model is made to a scale of  $s = 1/30$  which is the ratio of wave height to the water depth. In the wave flume, water depth and wave height are maintained at 1.40m and 40mm respectively. The wave generator is a plunger type capable of producing regular waves of time period 0.65-0.8s with the input values of plunger velocity 10 counts and stroke 1. White Polypropylene (PP) sheet is used to make floating plate model of dimension  $2\text{m} \times 0.5\text{m} \times 0.01\text{m}$  used for the experiment. The Polypropylene (PP) sheet has density  $0.91\text{g/cc}$ , Poisson's ratio 0.42 and Elasticity 1.5GPa. The PP plate is placed at a 7m distant from the wave generator. The plate is moored using thin ropes and zero tension in such a way that the lateral motion or drifting is arrested without affecting waves. A displacement sensor (DS) is placed just above the plate surface in order to capture wave induced deflection. When the waves pass beneath the plate, the plate deflects vertically due to which the needle fixed to the plate displaces and the displacement readings are recorded using Emcon wave recorder software. However, the displacement sensor (DS) cable is not long enough to extend to the middle of the flume. Hence, the deflection of the plate is found out by placing displacement sensor at different position on the plate for particular time period. Waves of the 0.7s time period are produced using wave generator and the deflections are

recorded using displacement sensor at every 200mm interval from the front edge of the plate. The experimental results are plotted in the Sub-section 4.2.

#### 4. Numerical computations

A numerical code has been developed in order to study the effect of different wave and structural parameters on the wave reflection, wave force acting on the barrier, barrier and plate deflection for various bottom profiles. The numerical computations are performed using  $h_1 = 10\text{m}$ ,  $h_3 / h_1 = 0.75$ , sloping parameter  $\theta_s = 45^\circ$ , incident angle  $\theta = 25^\circ$ , time period  $T = 8\text{s}$ , porous effect parameter  $G = 0.1 + 0.1i$ , the non-dimensional flexural rigidity of the barrier  $\gamma_b = EI_b / (\rho g h_3^4) = 0.1$ , non-dimensional compressive force  $\beta_b = Q / (\rho g h_3^2) = 0.1$ ,  $\alpha_b = m_b \omega^2 / (\rho g h_3^4) = 0.1$ , Plate's Young's modulus  $EI_p = 3\text{Gpa}$ , plate thickness  $t_p = 0.1h_3$ , plate density  $\rho_p = 917\text{kg m}^{-3}$ , water density  $\rho = 1025\text{kg m}^{-3}$  and acceleration due to gravity  $g = 9.8\text{m s}^{-2}$  are kept fixed in the whole computation unless otherwise mentioned. The reflection coefficient  $K_r$ , surface deflection  $\eta$  for  $j^{\text{th}}$  region, non-dimensional wave force acting on the flexible porous barrier  $F_b$  at  $x = x_2$ , are computed using the following formulae.

$$K_r = \left| \frac{R_0}{I_0} \right|, \quad \eta = i \frac{1}{\omega} \frac{\partial \phi_j}{\partial z} \Big|_{z=0} \quad \text{and} \quad F_b = \left| \frac{K_b}{\rho g h_1^2} \right| \quad \text{where} \quad K_b = i \rho \omega \int_{-h_3}^0 \{ \phi_4(x, z) - \phi_3(x, z) \} \Big|_{x=x_2} dz. \quad (26)$$

In the present study, various types of undulating bed profile function  $h_2(x)$  as in Eq. (27) (see Porter and Porter<sup>[45]</sup>) in the region 2 ( $0 > x \geq x_1 = L_1$ ), are considered.

$$h_2(x) = h_1 - b \left\{ 1 - \delta \left( 1 - \frac{x}{L_1} \right)^2 + (\delta - 1) \left( 1 - \frac{x}{L_1} \right) \right\}. \quad (27)$$

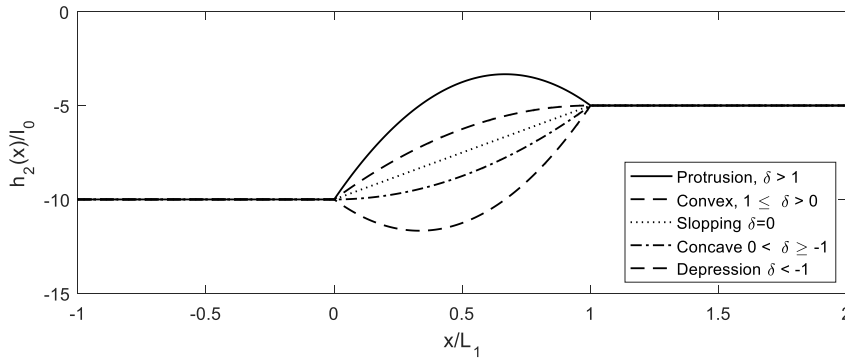


Fig. 5. Variation of bottom bed profiles  $h_2(x)$  for different values of  $\delta$  with  $h_1 = 10\text{m}$ ,  $h_3 = 0.5h_1$  and  $L_1 = 10h_1$ .



where  $b=(h_1-h_3)$  and  $\delta$  being a real number. The values of  $\delta$  give different kind of bed profiles as shown in Fig. 5. When  $\delta = 0$ , the function  $h_2(x)$  gives a linear sloping bed profile, if  $\delta > 1$ , the same function produces protrusion profile above the depth  $h_3$ .  $0 < \delta \leq 1$  and  $-1 \leq \delta < 0$  correspond to convex and concave profile respectively whilst  $\delta < -1$  produces depression in the bed profile as shown in Fig. 5. In the present study, while analyzing the effect of various parameters on the wave reflection, horizontal force on the barrier, free surface elevation and plate deflection,  $\delta = 1, 0, -1, -2$  were considered. However,  $\delta = 1$  is kept fixed in several cases unless mentioned otherwise. For clarity, wave interaction with floating elastic plate under various cases are analyzed in the subsequent different subsections.

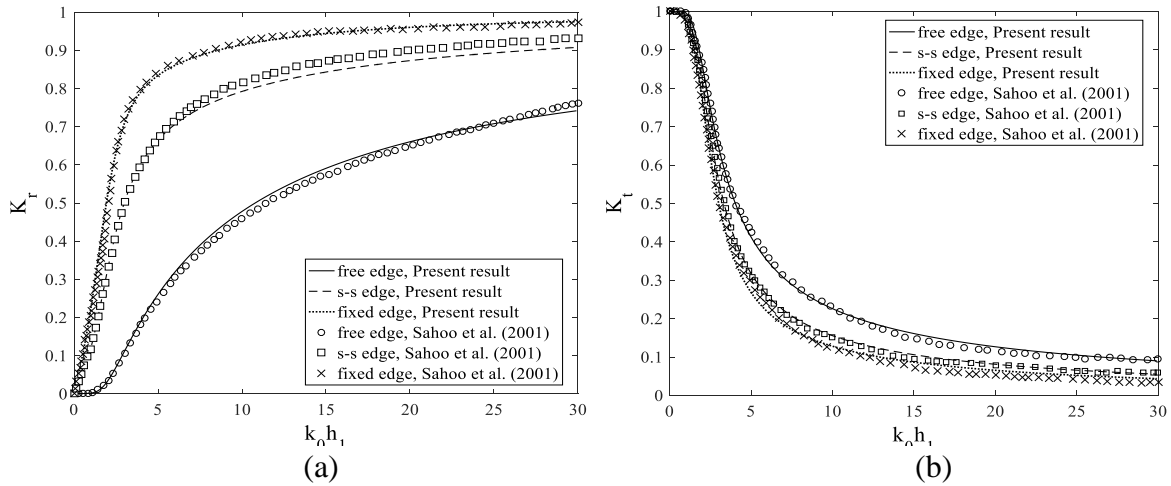


Fig. 6. Variations of wave reflection and transmission coefficients for  $\delta = 0$ , with  $h_1 = h_3$  and  $L_1 = 0$ .

#### 4.1. Floating semi-infinite elastic plate without presence of undulating bottom bed

In Fig. 6, the variations of wave reflection coefficients  $K_r$  and transmission coefficients

$K_t = \left| \frac{p_0 T_0 \tanh p_0 h}{k_0 I_0 \tanh k_{1,0} h} \right|$  without the presence of flexible porous barrier and undulating bottom bed, are

plotted. As discussed in Sec. 3.4.2,  $L_1$ ,  $L_2$  and  $L_3 = 0$  with  $h = h_1 = h_2$ , are considered to eliminate the undulating bottom and barrier from the present formulation. Hence, the plate covered region extends from the origin to the positive  $x$ -direction. Fig. 6(a), reveals that the highest and lowest wave reflections occur in the cases of fixed edge condition and free edge condition respectively. However, the reverse pattern in the transmission coefficient is observed in Fig. 6(b), which may happen due to the transmission of more wave energy in the case of free edge condition than fixed edge condition. The results are also compared with Sahoo et al. <sup>[3]</sup> in Fig. 6. In the present approach, the orthogonal properties of vertical eigenfunctions in the open water region, is used to solve the system of algebraic equations whilst Sahoo et al. <sup>[3]</sup> used the inner product of vertical eigenfunctions of the plated covered region to solve the problem. The good agreement of the present results with Sahoo et al. <sup>[3]</sup> implies the

correctness of the present approach and numerical computation.

#### 4.2. Floating finite elastic plate without the presence of undulating bottom bed

In this section, the numerical result computed from subsection 3.4.3, is compared with the experimental result in the case of floating finite elastic plate considering  $h = 30\text{m}$ , plate length  $L_p = 60\text{m}$ , wave height  $H_0 = 1\text{m}$  and plate thickness  $t_p = 0.01h$  with the same engineering properties of the plate that is used in the experiment. The plate deflection of the freely floating plate is measured in the wave tank experiment using the method described in subsection 3.4.3.

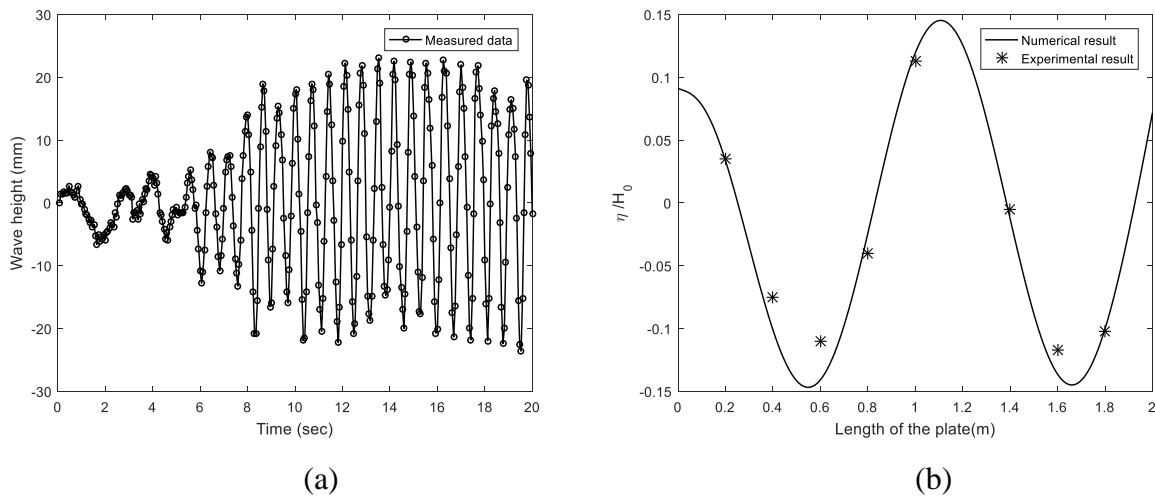


Fig 7: Variation of wave elevation recorded using wave probe (WP) and comparison of numerical and experimental results of the dimensionless plate deflection ( $\eta / H_0$ ).

In Fig. 7(a), the wave elevation recorded using wave probe (WP) is plotted. After analyzing Fig. 7(a), the average time period is considered as 0.7s and 40mm wave height is considered. Using the dispersion relation  $\omega^2 = gk \tanh kh$ , wave number is found out as  $8.212864\text{m}^{-1}$ . The time period of the model is converted to time period of prototype with the help of Froude's model law for numerical computations. Table 1 shows that wavelength is approximately same in both cases. Hence, both the results can be comparable. In Fig. 7(b), the experimental and numerical results are compared. In spite of the limitation of the wave maker, the figure reveals good agreement between the experimental result and the numerical results after normalizing with wave height 0.04m.

Experimental data	Numerical calculations
$k = 8.212864 = \frac{2\pi}{\lambda}$ $\lambda_{\text{experimental}} = 0.765 = \lambda_{\text{theoretical}} \times s$ $\lambda_{\text{theoretical}} = 22.95125m$	$k = 0.2737 = \frac{2\pi}{\lambda}$ $\lambda_{\text{theoretical}} = 22.956468m$

Tab 1: Wavelength calculation in experimental model scale

#### 4.3. Coupled finite floating elastic plate and Barrier system in the presence of undulating bottom bed

In this section, the system of equations Eq. (23), is solved for the finite elastic plate case in the presence of flexible porous barrier and undulating bottom. The length of the elastic plate is given by  $L_p$ . Sloping parameter  $\theta_s$  is introduced to describe the undulating length  $L_1 = (h_1 - h_3) / \tan(\pi\theta_s / 180)$ .

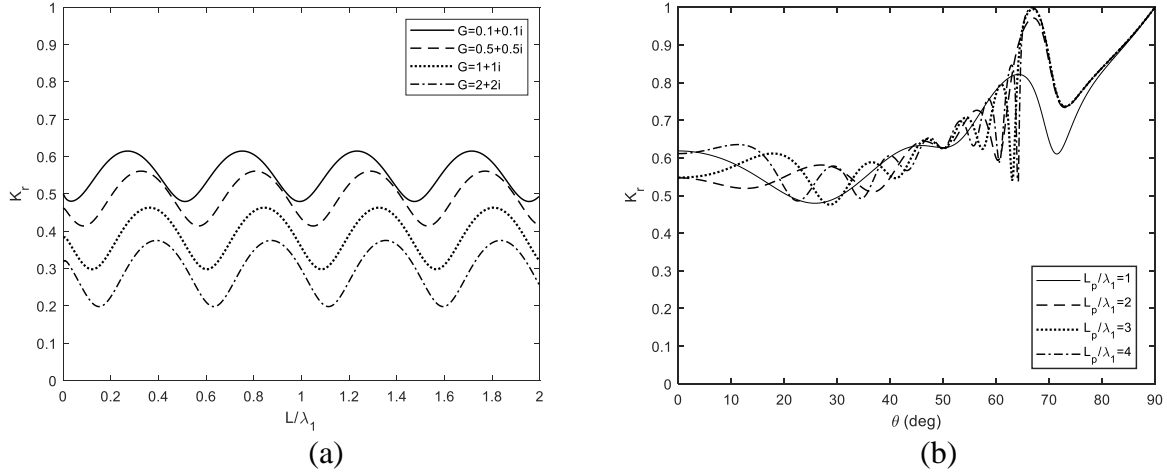


Fig. 8. Variations of reflection coefficients versus (a) non-dimensional wavelength for different value of porous effect parameter  $G$  with  $\delta = 1$  and (b) non dimensional plate length  $L_p / \lambda_1$  with  $\theta_s = 45^\circ$ , and  $G = 0.1+0.1i$ .

In Fig. 8(a), the variations of reflection coefficients versus non-dimensional wavelength for different value of porous effect parameter  $G$  is plotted. In general, maxima and minima of the reflection coefficients occur periodically. It can be observed that there is a right shift in the minima and maxima of these curves, which is due to the phase shift of the reflected wave as the length and profiles of the undulated region changes. Decrease in porous effect parameter, reduces the wave transmission due to the increase in friction, which results increase in wave reflection. In Fig. 8(b), the variations of reflection coefficients versus oblique incident angle for different values of non-dimensional plate length  $L_p / \lambda_1$  is plotted. The number of maxima and minima increases with the increase of plate length.

As the plate length increases, the maximum of these curves tends to attain full reflection around  $\theta_c = 65.7^\circ$ , which is referred as critical angle in Fig. 11(a) for the semi-infinite plate case.

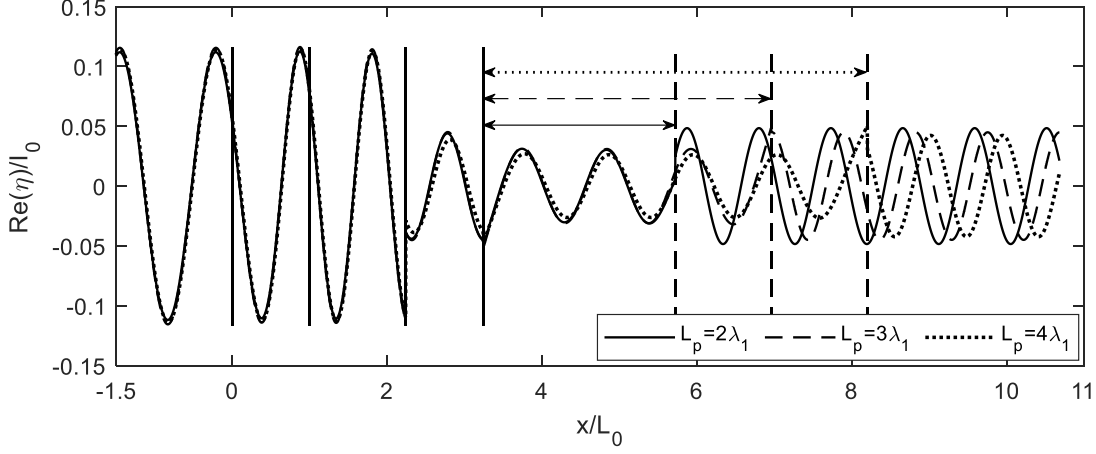


Fig. 9. Surface elevation for different values of elastic plate length  $L_p$ , with the presence of porous barrier with  $\delta = 1$ ,  $h_3 = 0.5h_1$ ,  $\theta = 0^\circ$ ,  $\theta_s = 5^\circ$ ,  $E_p = 3\text{GPa}$ , and  $L = 100\text{m}$ .

The surface elevation for different values of elastic plate length  $L_p$ , with the presence of porous barrier is shown in Fig. 9. It is observed that the amplitude of the transmitted wave decreases with the increase of plate length due to the increase of wave energy dissipation by the elastic plate due to deformation of the flexible structure.

#### 4.4. Coupled semi-infinite floating elastic plate and Barrier system in the presence of undulating bottom bed

In this section, the algebraic system Eq. (23) associated with wave interaction with coupled semi-infinite floating elastic plate and flexible porous barrier system in the presence of undulating bed profiles, is computed using finite difference scheme. In the subsequent figures  $L = (L_2 - L_1)$ , is used to non-dimensionalize wavelength  $\lambda_1$ .

In Figs. 10(a) and 10(b), the variation of wave reflection coefficients are plotted against non-dimensional wavelength  $L/\lambda_1$  for different values of undulating bed sloping parameter  $\theta_s$  and undulation parameter  $\delta$  respectively. In both of the figures, right shift is observed in the minima and maxima of these curves as in Fig. 10(a). On the other hand, with the increase in  $\theta_s$ , the undulated region length  $L_1$  decreases. The increase in sloping angle leads to step type bed profile while small  $\theta_s$  leads to near flat type bottom. Fig. 10(a) reveals that maxima in wave reflection increase with the increase in sloping angle due to increase in reflected wave. In Fig. 10(b), lowest wave reflection is

observed for sloping bed profile ( $\delta = 0$ ) due to comparatively less damping, while highest wave reflection is observed for depression bed profile ( $\delta = -2$ ). The figure depicts that for  $|\delta| > 1$ , wave reflection and phase difference, increase significantly.

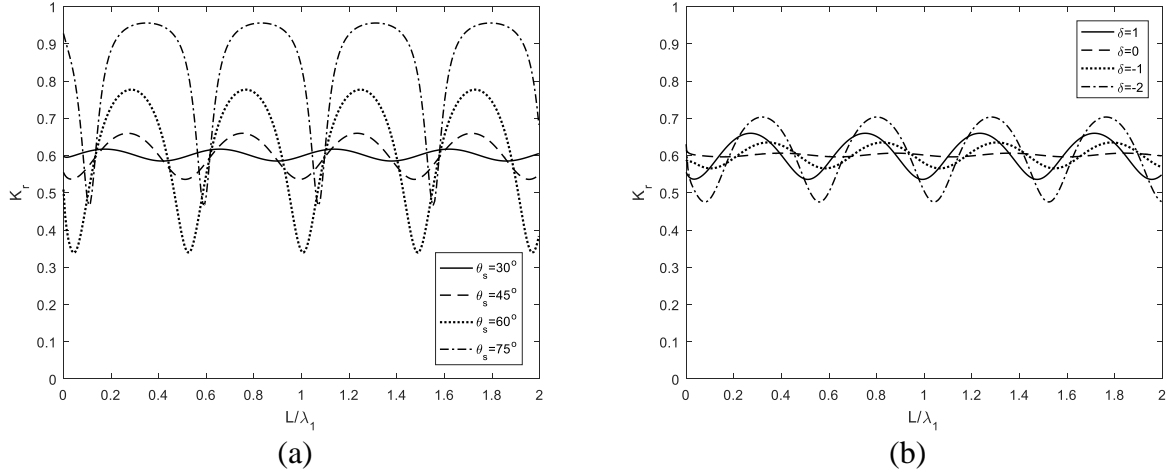


Fig. 10. Variations of reflection coefficients versus non-dimensional wavelength for different value of (a) sloping parameter  $\theta_s$  with  $\delta = 1$  and (b) undulation parameter  $\delta$  with  $\theta_s = 45^\circ$ ,  $\theta = 25^\circ$  and  $G = 0.1 + 0.1i$ .

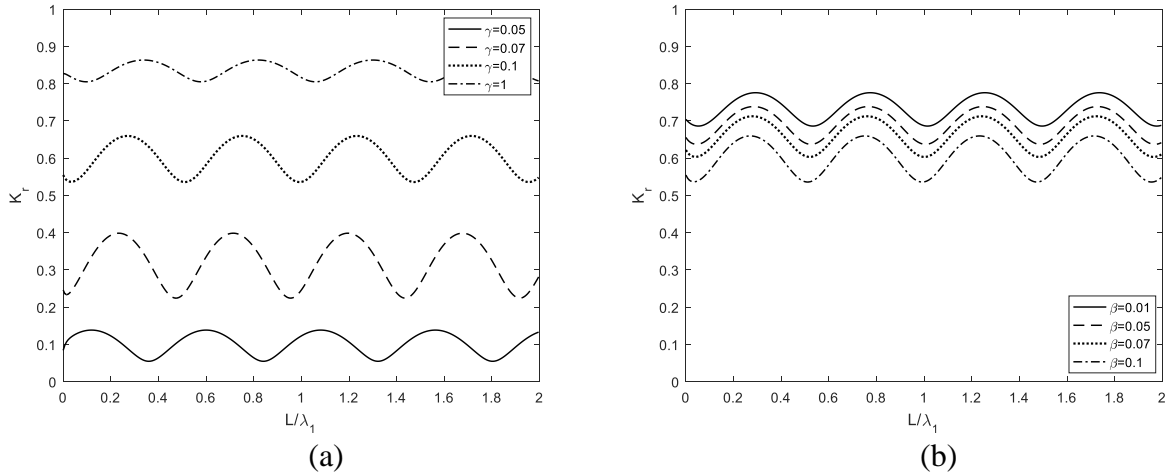


Fig. 11. Variations of reflection coefficients versus non-dimensional wavelength for different value of (a) flexural rigidity parameter  $\gamma_b$  and (b) compressive force parameter  $\beta_b$  with  $\delta = 1$ ,  $\theta_s = 45^\circ$ ,  $\theta = 25^\circ$  and  $G = 0.1 + 0.1i$ .

In Figs. 11(a) and 11(b), the variation of wave reflection coefficients are plotted against non-dimensional wavelength for different values of non-dimensional flexural rigidity parameter and compressive force respectively. From Fig. 11(a), it is observed that the wave reflection increases with the increase of flexural rigidity of barrier. This may happen due to the increase in momentum of the fluid as it interacts with a stiffer structure, which results in less wave to pass through the barrier. Fig.

11(b), reveals that the wave reflection decreases with the increase of compressive force acting on the flexible porous barrier. From Figs. 11(a) and 11(b), it is clear that structural rigidity influences the wave reflection significantly compared to the compressive force.

In Figs. 12(a) and 12(b), the variation of wave reflection coefficients are plotted against non-dimensional wavelength for different values of incident angle and water depth ratio respectively. From Fig. 12(a), it is observed that there is a right shifting of reflection minima. It also reveals that the reflection minima and the number of occurrences decrease with the increase of oblique incident angle. On the other hand, wave reflection increases with the decrease of water depth ratio due to the decrease in the length  $L_1$  and increase in  $\theta_s$  with fixed  $\theta$ . The number of occurrence of maxima and minima, increases with the decrease of depth ratio. It may be noted that the difference between maxima and minima reflection, increase with the increase of depth ratio.

In Fig. 13(a) and 13(b), the variation of wave reflection coefficients are plotted against incident angles for different values of  $L/\lambda_1$  and porous effect parameter  $G$  respectively. It is observed that full reflection occurs near  $\theta = 65.7^\circ$ , irrespective of  $L/\lambda_1$  and porous effect parameter  $G$ . The incident angle  $\theta_c = 65.7^\circ$  is referred as critical angle. In general, the wave reflection initially decreases rapidly with the decrease of incident angle up to certain extreme minimum value and then the wave reflection increases and attains full reflection at  $\theta_c$ . From Fig. 13(a), it is observed that after attaining full reflection, the wave reflection decreases further and maintains nearly

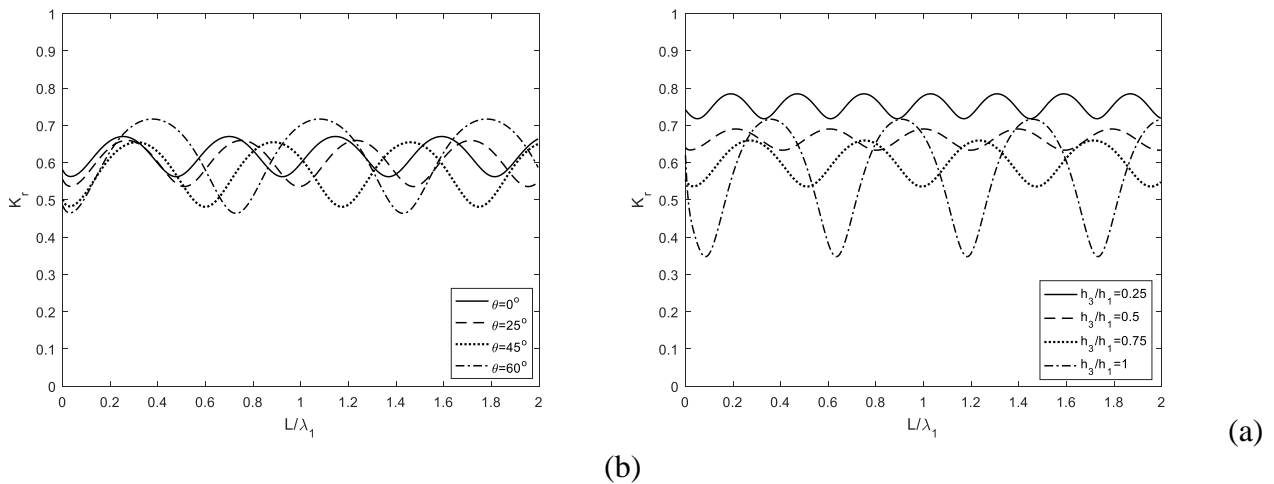


Fig. 12. Variations of reflection coefficients versus non-dimensional wavelength for different value of (a) obliquely incident wave angle  $\theta$  with  $h_3/h_1 = 0.75$  and (b) water depth ratio  $h_3/h_1$  with  $\delta = 1$ ,  $\theta_s = 45^\circ$ ,  $\theta = 25^\circ$  and  $G = 0.1 + 0.1i$ .

constant values for small incident angles. However, the oscillatory patterns of the wave reflection

increase with the increase of  $L/\lambda_1$ . In Fig. 13(b), with an increase of absolute value of porous effect parameter  $G$ , the wave reflection decreases due to the transmission of more wave energy through the flexible porous barrier. However, comparison with Fig. 11(a), reveals that not only flexibility but also moderate choice of porosity affects the wave reflection by the flexible porous barrier. This may be due to a part of the wave energy dissipates while passing through the barrier whilst another part deforms the flexible barrier.

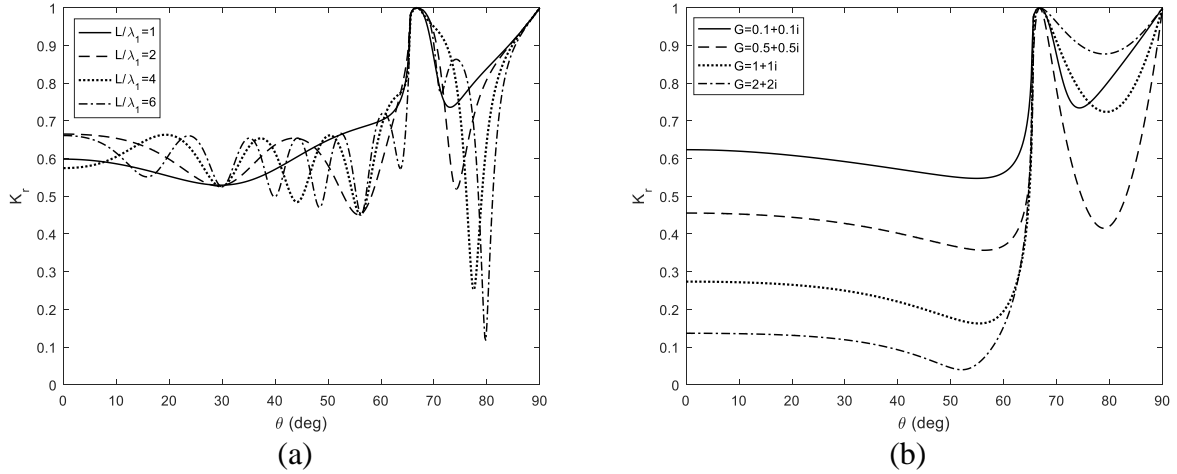


Fig. 13. Variations of reflection coefficients versus obliquely incident wave angle  $\theta$  for different value of (a) undulation parameter  $\delta$  with  $h_3/h_1 = 0.75$ ,  $G = 0.1+0.1i$  and (b) porous effect parameter  $G$  with  $\delta = 1$ ,  $\theta_s = 45^\circ$ , and  $L = 10\text{m}$ .

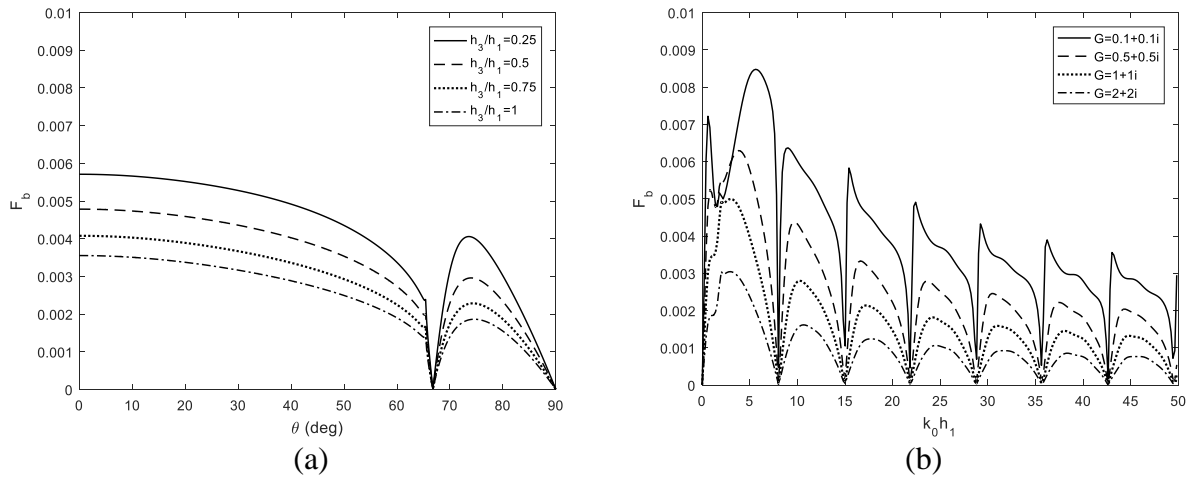


Fig. 14. Variations of non-dimensional wave force  $F_b$  versus (a) obliquely incident wave angle  $\theta$  for different values of water depth ratio  $h_3/h_1$ , with  $G = 0.1+0.1i$ . and (b) non-dimensional wave number  $k_0 h_1$  for different values of porous effect parameter  $G$  with  $\delta = 1$ ,  $\theta_s = 45^\circ$  and  $L = 10\text{m}$ .

In Fig. 14(a), the variation of wave force acting on the flexible porous barrier is plotted against incident angle for different values of depth ratio. It is observed that the wave force acting on the barrier increases with the decrease of depth ratio. The wave force increases rapidly and then vanishes at the critical angle  $\theta_c$  and full reflection occurs at that incident angle (see Fig. 13). However, for incident angle  $\theta < \theta_c$ , the wave force increases gradually. The variation of wave force acting on the flexible porous barrier against non-dimensional wave number, is shown in Fig. 14(b). It is observed that the wave force increases with the decrease of absolute value of porous effect parameter. With a comparison with Fig. 13(b), reveals that smaller absolute value of porous effect parameter produces higher reflection by allowing less wave to pass through the barrier, which results higher wave force acting on the flexible porous barrier. The maxima of wave force acting on the barrier, reduces exponentially with the increase of incident wavenumber. Multiple occurrence of zero force are observed in Fig. 14(b). The maxima and minima in wave force corresponds to the constructive interference and destructive interference respectively between incident and reflected wave in the confined region between undulating region and barrier. The shift in the maxima of the wave force corresponds to the phase shift of the wave as the porosity of the barrier changes. It is observed that the gap between the two consecutive minima, increases gradually as the wavelength decreases.

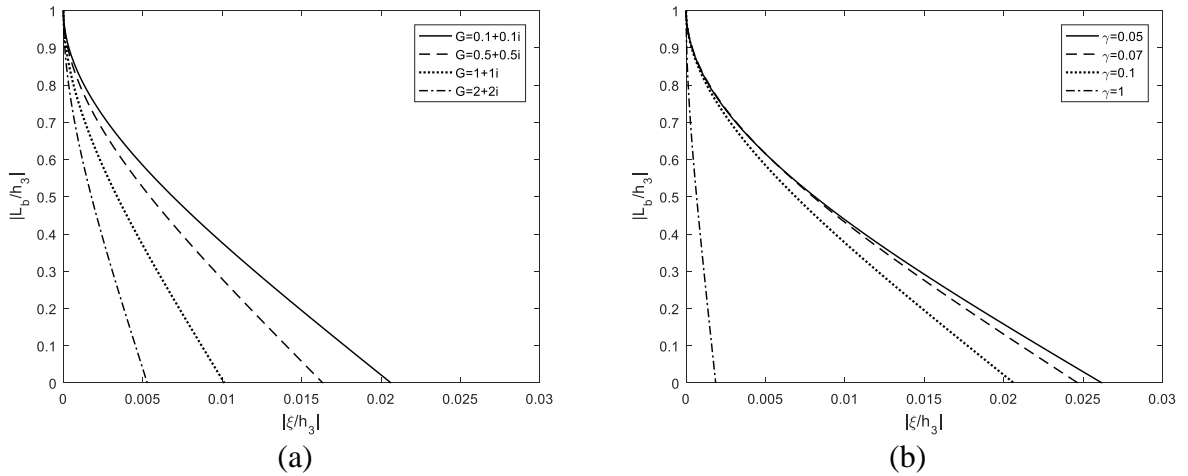
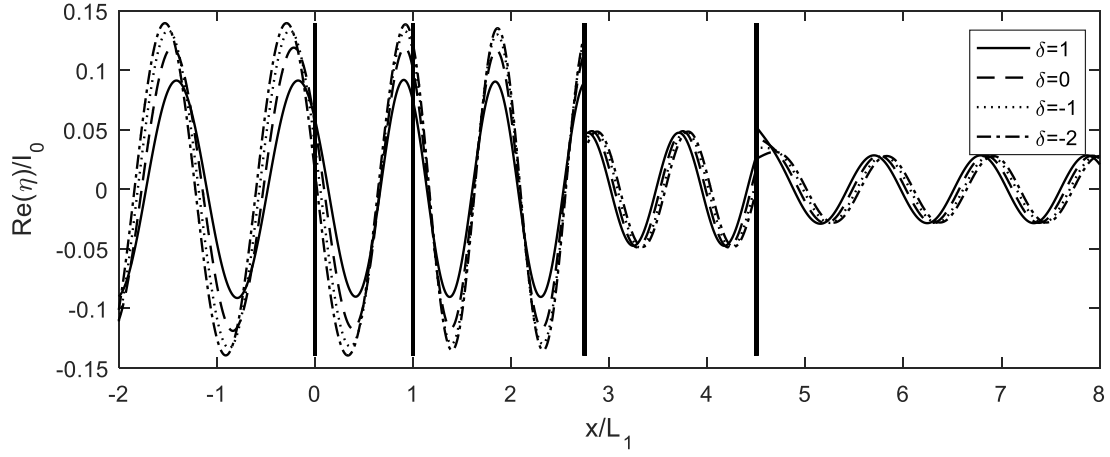
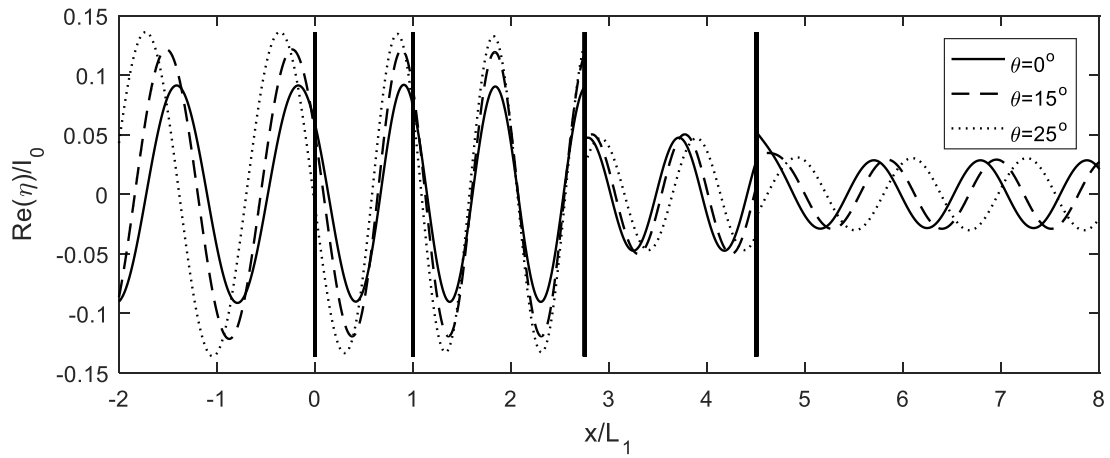


Fig. 15. Variations of non-dimensional plate deflection for (a) for different values of porous effect parameter  $G$  and (b) non-dimensional flexural rigidity  $\gamma_b$  with  $\delta = 1$ ,  $\theta_s = 45^\circ$  and  $L = 10\text{m}$ .

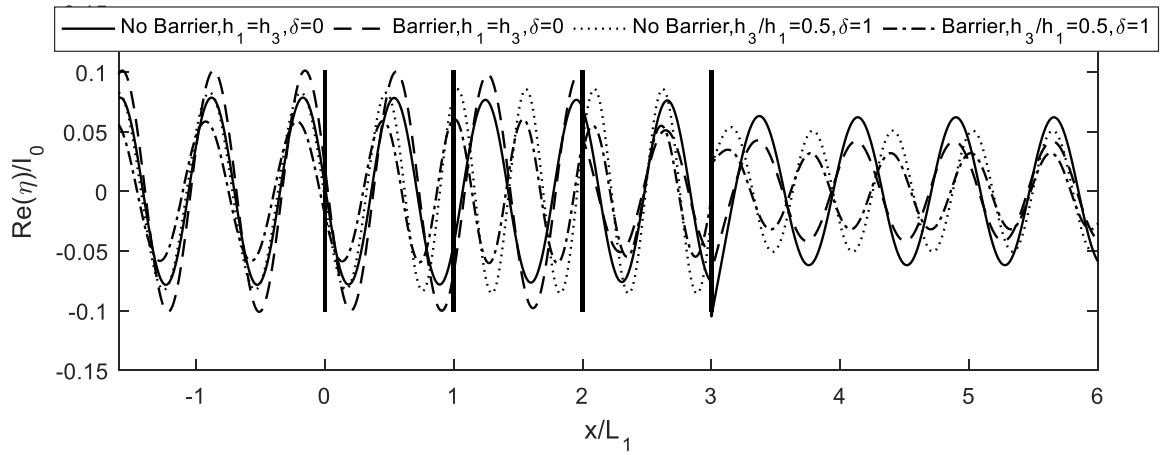




(a)



(b)



(c)

Fig. 16. Surface elevation for (a) different values of undulation parameter  $\delta$ , (b) different values of oblique angle  $\theta$ , (c) with and without presence of barrier with  $\delta=1$ ,  $h_3=0.5h_1$ ,  $\theta=0^\circ$ ,  $\theta_s=5^\circ$ ,  $E_p=3\text{GPa}$ , and  $L=100\text{m}$ .

Variation of dimensionless deflection of barrier ( $\xi/h_3$ ) is plotted in the Fig. 15 over dimensionless barrier depth ( $L_b/h_3$ ) for different values of (a) porous effect parameter and (b) flexural rigidity.

Generally, barrier deflection is maximum at free surface since the barrier is kept free at the free surface and fixed at the bottom. The barrier deflection increases rapidly near the free surface due to the highest concentration of energy at free surface. It is observed from Fig. 15(a), that the deflection of barrier reduces with the increase in the porosity parameter. High porous effect parameter leads to the passing more wave energy through the pores of the barrier, which reduce the wave load on the structure (see Fig. 14(b)) and less deflections occur. However, high porosity weakens the structure. In contrast to the Fig. 15(a), barrier deflections can be reduced with the increase in flexural rigidity of the barrier which is observed in Fig 15(b). In this case barrier is strengthened with increase in flexural rigidity, which may result in increase of wave load on the barrier. The moderate choice of porosity and flexural rigidity may lead to the effective design by avoiding both excess wave load and deflection of the barrier.

Fig.16 shows the variations of surface elevation with dimensionless length for different types of slopes, oblique incidence angle. Surface elevation in plate covered region represents the transverse deflection of the plate. The discontinuity in the elvation is observed at the location of barrier and at the interface of plate covered and free surface regions. It can be observed that the free surface elevation decreases in the presence of flexible porous barrier. In Fig. 16(a), shifting of maxima and minima of the plate deflections are observed with the change of undulating parameter  $\delta$ . For  $|\delta| > 1$ , the free surface elevation increases, which leads to comparatively less damping and higher wave reflection by the combine system. This phenomenon is shown in Fig. 10(b). In Fig. 16(b), the absolute value of free surface elevation increases with the increase of incident wave angle due to the increase in reflected wave. It is evident from the Fig. 16(b) that the plate deflection is reduced when the flexible porous barrier is placed before the plate and the presence of bottom undulations lead to further reduction of plate deflection.

## 5. Conclusions

In the present study, the surface gravity waves interaction with a floating elastic plate coupled with a flexible porous barrier in the presence of undulating bottom, is investigated. Two types of plate configurations are namely (a) finite plate and (b) semi-infinite plate studied. Eigenfunction expansion method and modified mild-slope equation are used to handle the physical problem. Finite difference scheme is used to solve modified mild-slope equation. The hydrodynamic forces acting on the barrier, the effect of different wave and structural parameters on the wave reflection and plate deflection for various bottom profiles, are evaluated in several cases. Periodic minima and maxima are observed in reflection coefficients due to presence of barrier. It is found that less wave reflection occurs for sloping bed profile compare to rest of the bed profile. It is observed that barrier deflection increases rapidly

near the free surface due to the highest concentration of energy. Both porosity and flexibility of the barrier significantly impact the wave reflection and reduce wave force by wave energy dissipation, which is a major advantage for developing an effective wave reduction system. It is observed that full wave reflection occurs for certain critical angle and wave force acting on the barrier vanishes for the same critical angle for the semi-infinite plate case while the wave reflection tends to attain minimum value for the finite case and these minimum value increases with the increase of plate length. The present study on the plate deflection reveals that positioning a barrier between plate and undulated region, indeed reduce the plate deflection and the presence of bottom undulations lead to further reduction of plate deflection. As special case, wave interaction problem with a finite floating elastic plate in the absence of barrier is studied experimentally and the experimental result has shown good agreement with the numerical result despite the limitations of the apparatus. The present study will be helpful in the design of marine structures to reduce wave impact on the very large floating structure.

**Funding:** Council of Scientific and Industrial Research (CSIR) (MLP 1701), Graduate Aptitude Test in Engineering (GATE) Fellowship (CE16S57010055).

**Conflict of Interest:** The authors doesnot have any conflict of interest.

**Acknowledgement:** SM is gratefull to Council of Scientific and Industrial Research (CSIR) for funding this work through MLP 1701. SK B is gratefull to Ministry of Human Resource Development, Government of India for providing Graduate Aptitude Test in Engineering (GATE)

(CE16S57010055) fellowship. The authors declare that they have no conflict of interest. This article bears NIO contribution number XXXX.

## References

- [1] Squire, V. A. Synergies between VLFS hydroelasticity and sea ice research [J]. *Intl J. Offshore Polar Engng.*, 2008, 18, 1-13.
- [2] Lawrie, J. B., Abrahams, I. D. An orthogonality relation for a class of problems with high order boundary conditions; applications in sound-structure interaction [J]. *The Quarterly Journal of Mechanics and Applied Mathematics*, 1999, 52 (2), 161-181.
- [3] Sahoo, T., Yip, T. L., Chwang, A. T. Scattering of surface waves by a semi-infinite floating elastic plate [J]. *Physics of Fluids*, 2001, 13 (11), 3215-3222.
- [4] Manam, S., Bhattacharjee, J., Sahoo, T. Expansion formulae in wave structure interaction problems [J]. *Proceedings of the Royal Society A: Mathematical, Physical and Engineering Science*, 2006, 462 (2065), 263-287.
- [5] Mondal, R., Mohanty, S.K. and Sahoo, T. Expansion formulae for wave structure interaction problems in three dimensions [J]. *The IMA Journal of Applied Mathematics*, 2011, 78(2), 181-205.

- [6] Mohapatra, S.C., Sahoo, T. and Soares, C.G. Interaction between surface gravity wave and submerged horizontal flexible structures. *Journal of Hydrodynamics*, 2018, 30(3), 481-498.
- [7] Hermans A.J. A boundary element method for the interaction of free-surface waves with a very large floating flexible platform [J]. *J Fluids Struct*, 2000;14:943–56.
- [8] Andrianov, A.I., Hermans, A.J. Hydroelasticity of a circular plate on water of finite or infinite depth [J]. *Journal of Fluids and Structures*, 2005, 20(5), 719-733.
- [9] Andrianov, A.I., Hermans, A.J. Hydroelastic analysis of a floating plate of finite draft [J]. *Applied Ocean Research*, 2006, 28(5), 313-325.
- [10] Tkacheva, L.A. The diffraction of surface waves by a floating elastic plate at oblique incidence [J]. *J Appl Math Mech*, 2004, 68(3), 425-436.
- [11] Watanabe, E., Wang, C.M., Utsunomiya, T. and Moan, T. Very large floating structures: applications, analysis and design [D]. *CORE report*, 2004, 2, 104-109.
- [12] Kohout, A.L., Meylan, M.H., Sakai, S., Hanai, K., Leman, P., Brossard, D. Linear water wave propagation through multiple floating elastic plates of variable properties [J]. *Journal of Fluids and Structures*, 2007, 23, 649–663.
- [13] Mohapatra, S.C., Ghoshal, R. and Sahoo, T. Effect of compression on wave diffraction by a floating elastic plate [J]. *Journal of Fluids and Structures*, 2013, 36, 124-135.
- [14] Wang, C.M. and Tay, Z.Y. Very Large Floating Structures: Applications, Research and Development [C]. *The Twelfth East Asia-Pacific Conference on Structural Engineering and Construction*, 2011, 1877-7058.
- [15] Ohmatsu, S. Numerical calculation method of hydroelastic response of a pontoon-type VLFS close to a breakwater [C]. In: Ertekin RC and Kim JW (eds), *Proc 3rd Int Wksp VLFS*, University of Hawaii at Manoa, Honolulu, Hawaii, USA., 1999, 2, 805-811.
- [16] Maeda, H., Washio, Y., Osawa, H., Sato, C., Ikoma, T., Onishi, Y., and Arita, M. Characteristics of hydroelastic responses for elastic floating structure with wave energy absorption system in waves [C]. *JASNAOE*, 2000, 15, 173-178.
- [17] Utsunomiya, T., Watanabe, E., Nakamura, N. Analysis of drift force on VLFS by the near-field approach [C]. *ISOPE*, 2001, 217-221.
- [18] Hong, D.C., Hong, S.Y., and Hong, S.W. Reduction of hydroelastic responses of a very-long floating structure by a floating oscillating-water-column breakwater system [J]. *Ocean Eng.*, 2006, 33(5-6), 610-634.
- [19] Wang, K.-H., Ren, X. Water waves on flexible and porous breakwaters [J]. *Journal of Engineering Mechanics*, 1993, 119 (5), 1025-1047.
- [20] Chwang, A. T. A porous-wavemaker theory [J]. *Journal of Fluid Mechanics*, 1983, 132, 395-406.
- [21] Yip, T., Sahoo, T., Chwang, A. T. Trapping of surface waves by porous and flexible structures [J]. *Wave Motion*, 2002, 35 (1), 41-54.

- [22] Lee, M., Chwang, A. Scattering and radiation of water waves by permeable barriers [J]. *Physics of Fluids*, 2000, 12 (1), 54-65.
- [23] Bhattacharjee, J., Guedes Soares, C. Oblique wave interaction with a floating structure near a wall with stepped bottom [J]. *Ocean Engineering*, 2011, 38(13), 1528-1544.
- [24] Lo, E. Y. M. Flexible dual membrane wave barrier [J]. *Journal of Waterway, Port, Coastal, and Ocean Engineering*, 1998, 124 (5), 264–271.
- [25] Karmakar, D., Bhattacharjee, J., Guedes Soares, C. Scattering of gravity waves by multiple surface-piercing floating membrane [J]. *Applied Ocean Research*, 2013, 39, 40-52.
- [26] Karmakar, D., Guedes Soares, C. Wave transformation due to multiple bottom-standing porous barriers [J]. *Ocean Eng.*, 2014, 80:50-63.
- [27] Xiao, L., Kou, Y., Tao, L., Yang, L. Comparative study of hydrodynamic performances of breakwaters with double-layered perforated walls attached to ringshaped very large floating structures [J]. *Ocean. Eng.* 2016, 111, 279-291.
- [28] Geng, B.L., Wang, R.Q. and Ning, D.Z. The wave absorption efficiency of multi-layer vertical perforated thin plates. *Journal of Hydrodynamics*, 2018, 30(5), 898-907.
- [29] Massel, S.R. Extended refraction–diffraction equation for surface waves [J]. *Coastal Eng.*, 1993, 19, 97-126.
- [30] Porter, D., Staziker, D.J., 1995. Extensions of the mild-slope equation [J]. *J. Fluid Mech.* 300, 367-382.
- [31] Chamberlain, P.G., Porter, D. The modified mild-slope equation [J]. *J. Fluid Mech.* 1995, 291, 393-407.
- [32] Bennetts, L.G., Biggs, N.R.T., Porter, D. The interaction of flexural-gravity waves with periodic geometries [J]. *Wave Motion*, 2009, 46 (1), 57-73.
- [33] Manam, S.R., Kaligatla, R.B. A mild-slope model for membrane-coupled gravity waves [J]. *J. Fluids Struct.*, 2012, 30, 173-187.
- [34] Athanassoulis, G.A., Belibassakis, K. A. A consistent coupled-mode theory for the propagation of small-amplitude water waves over variable bathymetry regions [J]. *Journal of Fluid Mechanics*, 1999, 389, 275-301.
- [35] Belibassakis, K.A., Athanassoulis, G.A. A coupled-mode model for the hydroelastic analysis of large floating bodies over variable bathymetry regions [J]. *Journal of Fluid Mechanics*, 2005, 531, 221-249.
- [36] Gerostathis Th., Belibassakis, K.A. and Athanassoulis G.A. 3D hydroelastic analysis of very large floating bodies over variable bathymetry regions [J]. *Journal of Ocean Engineering and Marine Energy*, 2016, 2, 159-175.
- [37] Zhu, S. Water waves within a porous medium on an undulating bed [J]. *Coastal Engineering*, 2001, 42(1), 87-101.

- [38] Behera, H., Kaligatla, R.B., Sahoo, T. Wave trapping by porous barrier in the presence of step type bottom [J]. *Wave Motion*, 2015, 57, 219-230.
- [39] Kaligatla, R.B., Tabssum, S., Sahoo, T. Effect of bottom topography on wave scattering by multiple porous barriers [J]. *Meccanica*, 2018, 53(4-5), 887-903.
- [40] Behera, H. and Ng, C.O. Interaction between oblique waves and multiple bottom-standing flexible porous barriers near a rigid wall [J]. *Meccanica*, 2018, 53(4-5), 871-885.
- [41] Koley, S., Kaligatla, R. B. and Sahoo, T. Oblique wave scattering by a vertical flexible porous plate [J]. *Studies in Applied Mathematics*, 2015, 135(1), 1-34.
- [42] Mandal, S., Behera, H. and Sahoo, T. Oblique wave interaction with porous, flexible barriers in a two-layer fluid [J]. *Journal of Engineering Mathematics*, 2016, 100(1), 1-31.
- [43] Yu, X., Chwang, A. T. Wave-induced oscillation in harbor with porous breakwaters [J]. *Journal of Waterway, Port, Coastal, and Ocean Engineering*, 1994, 120 (2), 125-144.
- [44] Wu, C., Watanabe, E. and Utsunomiya, T. An eigenfunction expansion-matching method for analyzing the wave-induced responses of an elastic floating plate [J]. *Applied Ocean Research*, 1995, 17(5), 301-310.
- [45] Porter, R., and Porter, D. Water wave scattering by a step of arbitrary profile [J], *Journal of Fluid Mechanics*, 2000, 411, 131-164.